energies

MDPI

Article

Impact of Combined Demand-Response and Wind Power Plant Participation in Frequency Control for Multi-Area Power Systems

Irene Muñoz-Benavente [1], Anca D. Hansen [2], Emilio Gómez-Lázaro [3], Tania García-Sánchez [4], Ana Fernández-Guillamón [1] and Ángel Molina-García [1,*]

1 Department of Electrical Engineering, Universidad Politécnica de Cartagena, 30202 Cartagena, Spain; irene.munoz.benavente@gmail.com (I.M.-B.); ana.fernandez@upct.es (A.F.-G.)
2 DTU Wind Energy, Technical University of Denmark, 4000 Roskilde, Denmark; anca@dtu.dk
3 Renewable Energy Research Institute and DIEEAC-EDII-AB. Universidad de Castilla-La Mancha, 02071 Albacete, Spain; emilio.gomez@uclm.es
4 Department of Electrical Engineering, Universidad Politécnica de Valencia, 46022 Valencia, Spain; tagarsan@die.upv.es
* Correspondence: angel.molina@upct.es; Tel.: +34-968-32-5462

Received: 15 March 2019; Accepted: 26 April 2019; Published: 4 May 2019

Abstract: An alternative approach for combined frequency control in multi-area power systems with significant wind power plant integration is described and discussed in detail. Demand response is considered as a decentralized and distributed resource by incorporating innovative frequency-sensitive load controllers into certain thermostatically controlled loads. Wind power plants comprising variable speed wind turbines include an auxiliary frequency control loop contributing to increase total system inertia in a combined manner, which further improves the system frequency performance. Results for interconnected power systems show how the proposed control strategy substantially improves frequency stability and decreases peak frequency excursion (nadir) values. The total need for frequency regulation reserves is reduced as well. Moreover, the requirements to exchange power in multi-area scenarios are significantly decreased. Extensive simulations under power imbalance conditions for interconnected power systems are also presented in the paper.

Keywords: wind integration; demand response; frequency control; ancillary services

1. Introduction

The integration of renewable energy sources into power system has stressed system operation by causing balancing resources to cycle more frequently, and generating ramps of critical steepness or duration. Flexibility requirements increase strongly in power systems with combined wind and PV (photovoltaics) contribution of more than 30% of total energy and a share of PV in the renewables mix above 20–30% [1]. Nowadays, more than 140 countries currently have renewable energy targets in place. For example, the European Union (EU) has set targets to achieve a 37% renewables share in overall energy use, which could lead to renewable power generation shares in the range of 51–68% [2]. Under this scenario, maintaining a close balance between generated and demanded active power becomes crucial to guarantee power system security and stability, keeping grid frequency within certain intervals—less than ±1% of the nominal value for European power systems [3]. Traditionally, conventional supply-side units are equipped with primary and secondary frequency control systems [4], using the demand-side response to restore the balance only under severe instability conditions [5].

The primary frequency control (PFC) operates locally by means of a governor to modify, around a set-point, the mechanical power input of the supply-side units based on the local frequency deviation [6]. This control system, also known as the droop control, is decentralized with a timescale up to low tens of seconds and an initial rate of change determined by the rotating mass inertia of the power system. A new power balance and frequency grid stabilization is usually achieved, but does not in itself restore the nominal frequency. The main purpose of secondary frequency control (SFC), also called Automatic Generation Control (AGC) from the supply-side, is to balance the total system generation by recovering the global grid frequency and power interchanges among neighboring areas to their set-point values [7,8]. These unintended frequency deviations require reliable and fast-acting controllers to recover the grid frequency. However, many Control Areas (CAs) still adopt a simplified approach in the design of AGC, i.e., the conventional controls—Integral (I), Proportional Integral (PI), and Proportional Integral Derivative (PID). Although these gain controllers are simple to implement, their performance is not always satisfactory, being usually slow and presenting a lack of efficiency in handling system nonlinearities [9,10].

Over the years, the demand-side contribution to the power system started gaining considerable attention as a measure to obtain frequency and voltage regulation. Increased attention has been focused on demand response (DR), strongly motivated by the remarkable penetration of renewables into current power systems, particularly at the distribution level [11]. Loads, such as Thermostatically Controlled Residential Loads (TCRLs), can shift their demand over certain time intervals without compromising their performance and services. In fact, some authors considered that over 40% of residential appliances are compatible with load control strategies [12]. For this reason, TCRLs can be considered as ideal to be used in dynamic DR strategies [13,14]. Moreover, taking into account the large number of consumers and hence small loads connected to the grid, these strategies would improve resource utilization and subsequently would reduce supply-side capacity requirements [15]. Advantages and drawbacks of different load control and dynamic demand can be found in [16].

Most contributions in the last decade have proposed switching-off/on actions applied on TCRLs when frequency variations exceed certain limits [17–24]. However, these works have been mainly focused on PFC. In [17], a simple and optimal control strategy is proposed to modulate the customer load as a linear function of the frequency excursions. Short et al. [18] analyzed how a certain degree of frequency stability could be achieved by integrating dynamic demand controllers into fridges/freezers. These devices monitor the grid frequency and switch-off/on appliances accordingly, while achieving a trade-off between appliance requirements and the grid. Scenarios with high penetration of wind energy are also discussed. Samarakoon et al. [19] described a frequency-based load control scheme for primary frequency response purposes by using smart meters. Loads are grouped according to their relevance for the customer. When the grid frequency falls below the nominal value, each load controller is switched-off for a specific time depending on the frequency excursion. In [20], an experimental platform is proposed by using commercially available smart meters. These appliances are remotely controlled through smart sockets to evaluate the load blocking strategies. In [21], a decentralized approach for using TCRLs is proposed. The authors affirmed that a two-way communication between loads and the control center is not essential when the number of individual loads is considerably large. The value of Dynamic Demand (DD) concept is quantified in [22], enabling domestic refrigeration appliances to contribute to primary frequency regulation through an advanced stochastic control algorithm. In [23], a comprehensive central DR algorithm for primary frequency regulation is described in a smart micro-grid. Contributions for transient studies can be found in [24], where a systematic method to re-balance power and resynchronize bus frequencies after a disturbance with significantly improved transient performance is described. Recently, we discussed DR strategies applied to PFC by including auxiliary frequency control carried out by Wind Farms (WFs) [25]. The work focuses on evaluating the two control actions counteracting frequency deviations as well as their compatibility.

During the last years, the high integration of wind resource into the global energy mix has required an important reformulation of wind power plant services, including their contribution to the frequency

control [26,27]. These requirements are regularly updated and often include very rigid criteria, particularly in power systems with a relevant presence of wind power plants, where difficulties in maintaining the grid frequency within an acceptable range emerge as an additional concern under large wind power fluctuations [28,29]. In addition, some authors affirmed that the WT inertia contribution to the total kinetic energy stored in the power systems is considerably less significant than traditional power plants [30,31] and, subsequently, larger frequency deviations will be suffered by the systems after sudden generation or demand variations [32]. Moreover, systems with reduced total inertia experience a sharper immediate frequency drop under imbalance and, thus, are more vulnerable and sensitive to involuntary under-frequency load shedding [33]. Due to this scenario, alternative resources connected to the grid, mainly PV solar installations and wind power plants, are required to provide ancillary services [34]. With this aim, a frequency-dependent control loop is proposed in [35] for Variable Speed Wind Turbines (VSWTs) to improve frequency response and provide an active contribution to the frequency control. This additional controller synthesizes virtual inertia for VSWTs —i.e., kinetic energy stored in their rotating masses—that can be provided at the beginning of a frequency deviation event, diminishing its impact [35]. In this way, Spanish wind power plants are able to participate in ancillary services by a regulation framework issued by the Spanish Secretary of State for Energy [36], which made it legally possible since February 2016.

By considering previous works, this paper analyzes the demand-side contribution to SFC as an additional support to the frequency control strategy proposed in [21,25]. In line with these previous works, a decentralized demand-side solution is proposed to avoid the cost and complexity associated with two-way communications between many loads and the control center. The frequency-responsive load controller is thus extended by considering an additional integral-action function. This function adjusts the thermostat temperature of thermostatically controlled loads based on local frequency estimates. As a result, their power demand profiles are restructured, thus achieving a reduction (or increase) of their energy consumed. In this way, the controller is able not only to modify load's instantaneous power consumption, but also their energy demand during a specific time interval. This innovative load controller operates autonomously and provides a decentralized solution where individual loads are randomly distributed and connected to the grid. A two-area interconnected power system is simulated under severe wind power fluctuations to assess the proposed decentralized solution. An auxiliary frequency controller for VSWTs is also included to combine the contribution of VSWT's inertia to maintain the balance in future power systems with high wind power plant integration.

The rest of the paper is structured as follows: the implemented two-area interconnected power system is described in Section 2, including WF and demand-side modeling. The contribution of demand-side to SFC is discussed in Section 3. Extensive results are provided and widely discussed in Section 4. Finally, the conclusion is given in Section 5.

2. Power System Modeling: Wind Power Plant and Demand-Side Contribution to Frequency Control

2.1. Preliminaries

For studying the dynamic response of power systems dealing with frequency variations, traditional system modeling has been based on the following per unit (pu) expression [5]:

$$\Delta P_G - \Delta P_L = D\Delta f + 2H\frac{d\Delta f}{dt}, \quad (1)$$

where $\Delta P_G - \Delta P_L$ is the power imbalance, Δf is the difference between instantaneous and nominal system frequency and D, referred to as the damping factor, is the load dependence on frequency. Assuming that grid frequency can be considered as constant over large interconnected areas, the generating units can be then combined into an equivalent rotating mass M (being $M = 2H$

and H the inertia constant expressed in seconds). Likewise, loads are grouped and considered as an equivalent load, being D their equivalent damping factor [37].

For multi-area analysis purposes, the previous expression can be extended to different areas. With this aim, Figure 1 shows a general scheme of two-area interconnected power system, including primary and secondary frequency control by conventional generation units. This multi-area general scheme is considered in this paper, where a grid frequency and a system dynamic response characterizes each area. A high-impedance (elastic) transmission line is proposed to connect both areas [5]. Conventional generating units—highlighted with dashed lines—are modeled by considering Generation Rate Constraint (GRC) and speed Governor Dead-Band (GDB). The GRC is modeled by considering an "open loop" method and by adding two limiters bounded by ± 0.0017 (pu/s) within the generating units [38]. The GDB is defined as the total magnitude of a sustained speed change within which there is no change in the turbine valve position. The GDB transfer function model can be found in [38], assuming that the GDB of the 0.06% backlash type can be linearized in terms of change and the rate of change in the speed. Under the presence of certain nonlinearities and constraints, such as GRC and GDB, system dynamic responses can present significant overshoots and long settling times for frequency and tie-line power oscillations [39,40].

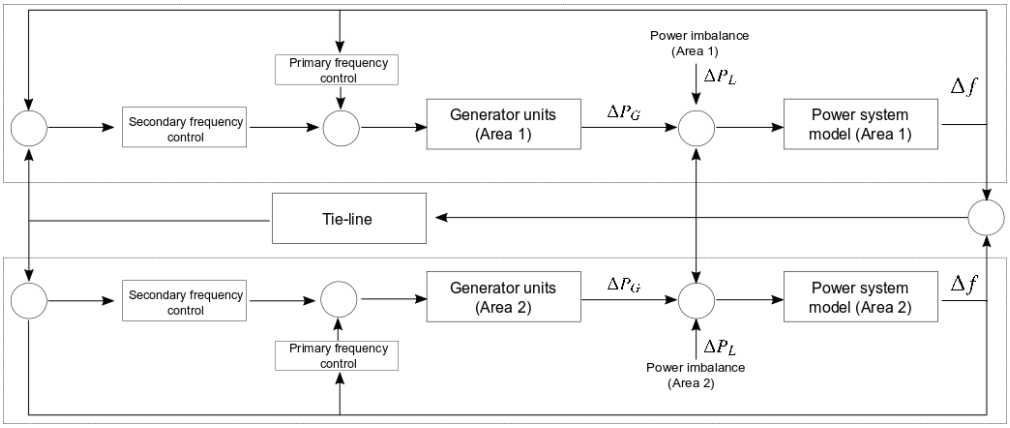

Figure 1. General scheme of two-area interconnected power system.

If one area is under power imbalance, the governor control mechanisms of both areas modify the power system to recover power balance. Grid frequency deviation, Δf, is used as input signal for primary and secondary frequency control. PFC is performed locally at the generator, being the active power increment/decrement proportional to Δf through the speed regulation parameter R, defined as the ratio of ΔP and Δf. Power flow control at the tie-line and damping of tie-line power oscillations are required for effective active power generation and frequency control. In this respect, SFC involves an integral controller modifying the turbine set-point of each area. A linear combination of both tie-line power errors between neighboring areas, $\Delta P_{tie,ij}$, and local frequency variations in each area, Δf_i, is used as the input to the corresponding integral controllers, which is called the Area Control Error (ACE) [41]. ACE in each area is then defined as follows [41]:

$$ACE_i = \sum_{j=1}^{n} \Delta P_{tie,ij} + \beta_i \Delta f_i, \tag{2}$$

where the suffix i refers to the CA and j to the generator number; β_i is the bias coefficient; f_i is the grid frequency of the i-CA; and $\Delta P_{tie,ij}$ is the actual value of the interchange power between i-CA and j-CA. Further information regarding tie-line bias control applicability to load frequency control for multi-area interconnected power systems can be found in [42]. The dynamic performance of the AGC

system thus depends on frequency bias factor β_i, in MW/Hz, and the integral controller gain value K_I. Optimal values of K_I and β are estimated by means of an Integral Squared Error (ISE) technique,

$$ISE = \int_0^T \left(\Delta P_{tie}^2 + (\beta_1 \Delta f_1)^2 + (\beta_2 \Delta f_2)^2 \right) dt, \quad (3)$$

where Δf_1 and Δf_2 are frequency deviations in Areas 1 and 2, respectively [43,44]. According to the specific literature, two different power systems were simulated: *(i)* the two-area interconnected power system proposed in [10]; and *(ii)* a two-area wind farm integrated power system based on [43–45]. Figure 2 depicts the initial two-area interconnected power system considered for the simulation by including the corresponding block diagrams.

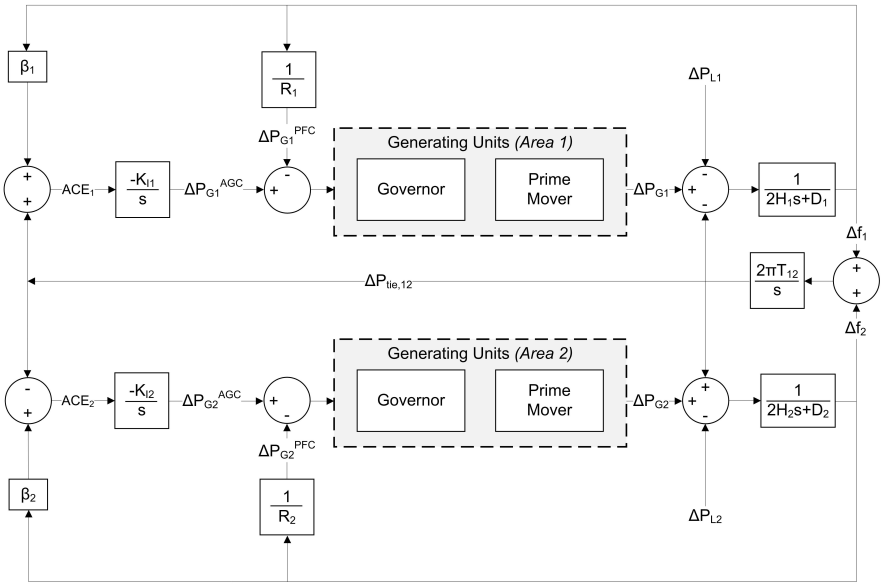

Figure 2. Block diagram of two-area interconnected power system.

2.2. Wind Power Modeling

Accounting for the relevance of wind power integration, two WFs containing VSWTs are explicitly considered in the power system model. Averaged time-varying wind speed profiles are applied to both wind power plants to evaluate wind active power fluctuations on grid frequency stability.

Primary frequency response of WFs is improved by including an additional inertia controller. This controller allows VSWTs to contribute to the system inertia through an active power regulation under frequency deviations [25,35],

$$P_{el}^{correction} = k_{\mathrm{WFs}} \cdot \frac{I_{\mathrm{WT}}}{2} \frac{df}{dt}, \quad (4)$$

where k_{WFs} is the virtual inertia factor and I_{WT} is the WT inertia (pu). Larger k_{WFs}-factors would improve WT contribution, maintaining WT rotational speed values within acceptable ranges. Figure 3 shows this additional virtual controller depending on the RoCoF (df/dt). An additional control loop that synthesizes virtual inertia is implemented for the VSWTs to contribute to the system's total inertia and thus to the system frequency control. The output power of the WF, $P_{el_{(pu)}}^{ref}$, is modified by an additional power $P_{el_{(pu)}}^{correction}$ depending on the RoCoF, df/dt, [30,46]. The global power of the WFs ($\Delta P_{WFs_{(pu)}}$) depends on the number of WT (N_{WTs}) and the VSWTs power set-point ($P_{0,WT}$) [47,48]. The proposed approach is thus based on a modified inertial control scheme, involving quick response through power-electronic circuits and subsequently providing frequency support from the rotational mass kinetic energy.

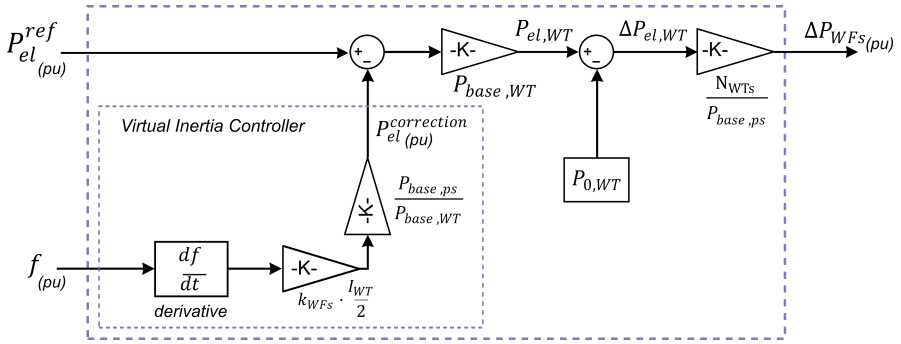

Figure 3. Virtual Inertia Block (VIB) diagram of the virtual frequency controller.

2.3. Demand-Side Modeling

Even thoguh demand-side was initially considered as non-controllable, nowadays, most authors agree with the idea that the devices can be categorized into controllable or uncontrollable [49]. Controllable loads are then defined as the loads suitable for deferral or shifting their power demand to off-peak periods without harming household's convenience, such as heating, ventilation, and air conditioning [50,51]. Because of their thermal properties, these devices can adapt their operation through on/off signals without adversely affecting their temperature requirements. The rest of the loads are considered uncontrollable, i.e., their use is completely determined by the end user. Assuming uncontrollable loads to be modeled by an equivalent load, their global power depends on frequency excursions through parameter D (equivalent damping factor), as discussed in Section 2.1.

In the proposed solution, controllable loads are modeled individually taking into account that their individual power demand can be modified by the following controllers: *(i)* a proportional frequency-dependent controller able to modify the active power demanded by the device and thus emulating PFC from supply-side; and *(ii)* an integral-action controller able to modified the thermostat individual load settings based on the ACE signal. The proportional frequency-dependent controller was previously described by the authors and discussed in [21,25]. This approach modifies the controllable load demand through forced switching-off/on actions. To operate under forced disconnections, frequency excursions exceed a predefined threshold, Δf, for a certain time (see Figure 4). Larger frequency deviations imply faster frequency control responses, thus entering the *Control Region*. Small frequency changes are maintained during longer time intervals, delaying the controller actions. Figure 4 also gives an example of Δf*-time* feature for a given load and its corresponding demand profiles in the event of a linear under-frequency excursion. As can be seen, when Δf*-time* boundaries are exceeded, load is forcibly switched-off for a predefined time period (*OFF-forced*). After a short recovery interval of forced connection (*ON*) to maintain the temperature within an acceptable range, and given that the frequency does not recover its rated value thus continuing within the *Control Region*, the load controller restarts a new cycle of forced disconnection. These *ON-* and *OFF-forced* time periods are designed keeping both appliance requirements in view and considering temperature limits that may be almost imperceptible by the customers. Actually, most controls for conditioning spaces and typical thermostat-controlled devices operate on a time scale of 10–15 min [52], which is in line with the SFC timescales. The proposed integral-action controller is thus based on thermostat temperature changes according to comfort level constraints and the expected demand-side contribution to SFC. Further discussion about thermal inertia, heat–cool flow rates and SFC can be found in Section 3.

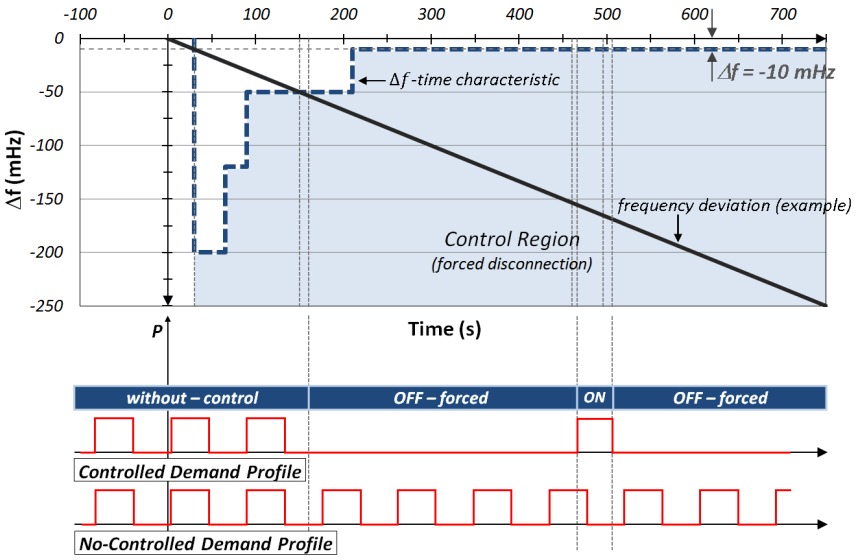

Figure 4. Frequency-responsive load controller: example of demand-side contribution to PFC and Δf-*time* characteristic.

Figure 5 shows an extended block diagram by including wind power generation frequency control (ΔP_{WFs}) and demand-side contribution to PFC and SFC considered in Area 1 (ΔP_{DS}^{SFC}). As can be seen, supplementary power due to wind power generation frequency control, ΔP_{WFs}, is added to the conventional generation response (prime movers), ΔP_{G1}, to provide an additional generation to the supply-side. The demand-side contributions to PFC and SFC are referred to as $\Delta P_{DS}{}^{PFC}$ and $\Delta P_{DS}{}^{SFC}$, respectively. This multi-area power system model is an extension of the block diagram depicted in Figure 2, by including frequency control to both supply-side—wind power plants—and demand-side.

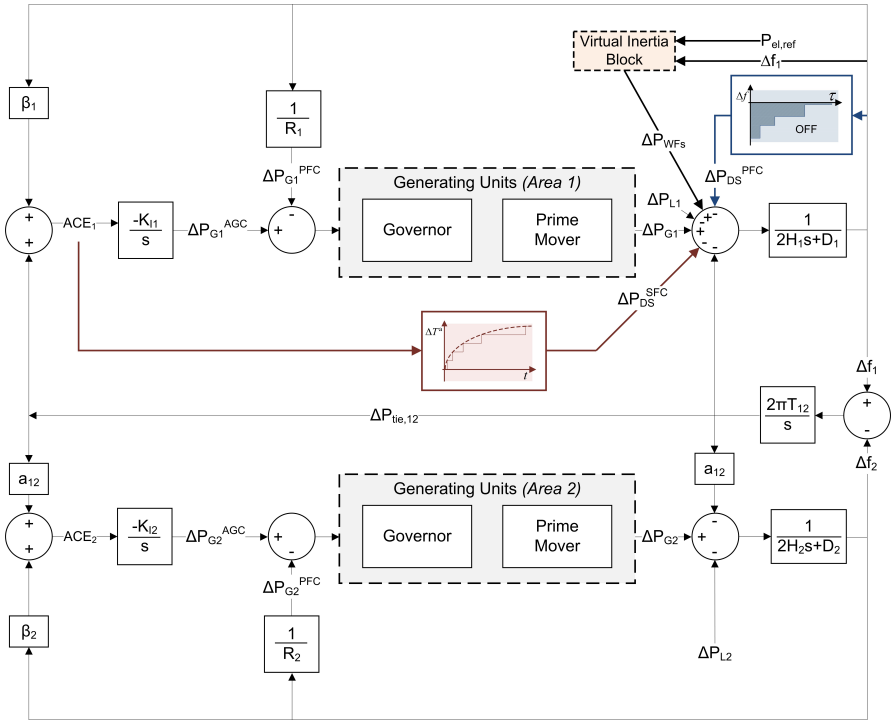

Figure 5. Two-area interconnected power system. WF and demand-side contribution to frequency control.

3. Demand-Side Contribution to SFC: Proposed Solution

3.1. General Description

The implementation of demand-side contribution to SFC is based on adding an integral-action function on the frequency controller proposed by the authors in [25]. By considering two or more areas, this integral-action controller gives a proportional value in line with the accumulated ACE of the corresponding area, i.e., the linear combination of both tie-line power errors (ΔP_{tie}) and local frequency excursions (Δf),

$$\Delta T_{set-point} = k \int (\Delta P_{tie} + \beta \Delta f) dt, \tag{5}$$

where k-parameter (constant of proportionality) is estimated depending on the expected frequency deviations (Δf), the time interval remaining, the frequency excursion and the comfort level ranges allowed by the customers. Figure 6 shows the controller block diagram implemented in *Matlab-Simulink* environment.

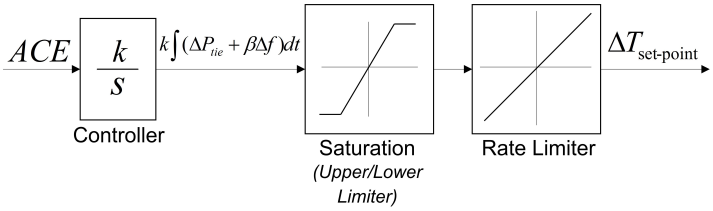

Figure 6. Demand-side contribution to SFC: controller block diagram.

Assuming that controllable loads operate according to their thermostat settings, TCRLs' normal operation patterns are then modified by changing their temperature set-points, $\Delta T_{set-point}$. Recovery to grid frequency deviations can be achieved by removing the residual steady-state error according to both AGC from the supply-side and Equation (5) from the demand-side. Communication is thus needed between the dispatch center and appliances when two or more areas are considered in the power system model. Recent contributions evaluate the impact on power system dynamic of errors in AGC systems [53]. Further discussion can be found in Section 3.2.

3.2. Implementation of Integral-Action Controller

For selecting the optimal value of k-parameter, three variables are considered. (i) *frequency deviation*: According to the European Standard EN–50160 [54], it is stated that the nominal value of grid frequency in most European countries, Asia and Africa is 50 Hz. It also provides the acceptable ranges for frequency variations: for interconnected supply systems under normal operating conditions, the averaged value of grid frequency measured over 10 s must be within a range of ±1% (49.5–50.5 Hz) for 99.5% of a week [55]. The proposed frequency control responses proportionally to the severity of the frequency excursion, and thus a proportional number of loads are called to switch-on/off depending on the frequency excursion to avoid undesirable over-frequency values. Subsequently, the number of loads is proportionally distributed taking into account that 100% of loads are required to support frequency control when the deviation is higher than 500 mHz and then grid frequency is kept within a range of ±1% (49.5–50.5 Hz), as previously commented. (ii) *duration of the frequency deviation*: The frequency deviation is considered to remain for at least 5 s, to be in line with the frequency excursion events emulated in the aforementioned contributions. (iii) *maximum allowable temperature variation for the thermostat set points*: Firstly, controllable loads are categorized into different groups according to their usage patterns and load profiles: *(Load-Group I)* including fridges/freezers; *(Load-Group II)* with air-conditioners/heat pumps; and *(Load-Group III)* corresponding to electric water heaters that have a great potential to store energy in advance [56]. In [57], load profiles of selected major household appliances in the U.S. are discussed in detail. When considering *Load-Group I*, and on the basis of technical specifications from different appliances manufacturers, the maximum allowable

temperature variation range for the fridge/freezer thermostat set point is set to +2 °C. For *Load-Group II*, air-conditioners/heat pumps, a variation range of ±3 °C is assumed acceptable for the customers, i.e., +3 °C for cooling mode and −3 °C for heating mode. Examples of cooling devices in demand response can be found in [58]. Finally, −6 °C temperature variation range is considered for *Load-Group III*. Hence, *k*-parameters are determined separately for each individual group of loads as follows:

$$\begin{pmatrix} k_{\text{ Load-Group I}} & = -0.8\ ^{\circ}\text{C}(\text{Hz}\cdot\text{s}), \\ k_{\text{ Load-Group II}} & = -1.2\ ^{\circ}\text{C}(\text{Hz}\cdot\text{s}), \\ k_{\text{ Load-Group III}} & = +5.0\ ^{\circ}\text{C}(\text{Hz}\cdot\text{s}). \end{pmatrix} \tag{6}$$

The value of *k* is thus estimated taking into account tolerances of the various frequency excursion phenomena that may occur on the mains (almost 95% of cases included). However, given the potential variability of the frequency deviations, in both magnitude and duration, the output of the integral-action controller needs to be limited. For example, in the case of large generation outages, the frequency deviation occurs too rapidly for the frequency containment reserves to be effectively activated and prevent the frequency from reaching values below and above these tolerances. This situation would cause the controllers to order unacceptable changes for temperature set points. For this reason, upper and lower saturation limits and rising and falling slew rates are included in the implemented model. Additionally, to avoid a synchronized and massive response of the loads, and consequently undesired frequency oscillations, a linear density probability function is implemented on each load controller to decide in a distributed manner when an individual load participates (or not) in the demand-side response. Therefore, the percentage of controllable loads varies gradually depending on the severity of the frequency excursion, and thus emulating proportional response of classical turbine-generator governors subjected to under-frequency excursions. The load decision to be involved in frequency control (or not) is then determined individually by each controllable load attending to: (i) the frequency excursion along the time; (ii) the severity of such frequency deviations (the more severe is the frequency excursion, the higher is the number of controlled loads to participate in the demand response); and (iii) the own load thermal characteristics that are in line with the off-time period ranges allowed by the customers. The decentralized solution can thus be used for practical applications, in which it may need a huge number of appliance switches.

Figure 7 shows both thermal and power demand response of controllable loads subjected to an under-frequency event. Their power demand profiles are also included by considering the load controller proposed in Section 3.1. The thermal set-point value is modified according to Equation (5). In this case, we consider $\Delta P_{tie} = 0$, and, thus, $\Delta T_{set-point}$ is estimated proportional to the accumulated deviation between the reference grid frequency and the measured value, according to Equation (5). $\Delta T_{set-point}$ represents the command sent by the individual load controller to the appliance after applying upper/lower and ramp limiters. As can be seen, within the first 25 s after the disturbance, the ramp slope is limited to a maximum rate of 0.08 °C per second. At the end of the simulation, the maximum temperature variation is limited to 2 °C. Moreover, this command has also been discretized in steps of 0.5 °C, i.e., $\Delta T_{set-point}$ *discretized*. The larger is the variation of the temperature set point, the lower is the duty-cycle of the load, thus decreasing power consumption and relieving power system reserves.

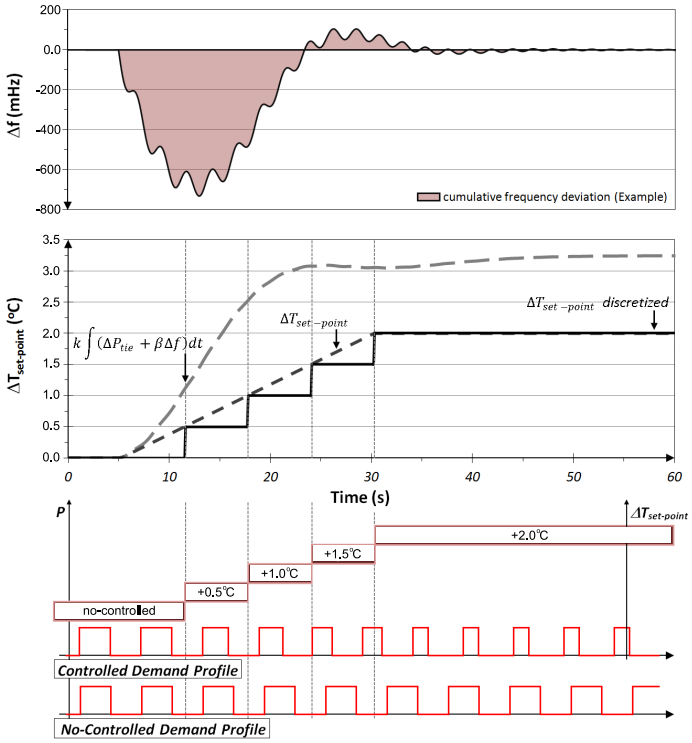

Figure 7. Frequency-response load controller: example of demand-side contribution to SFC.

4. Simulation and Results

4.1. Preliminaries

The most relevant data of the two implemented power systems were referred to an output power of 1200 MW and 1000 MW, with grid frequency nominal values of 50 and 60 Hz, respectively. In reference to wind power generation, both wind power plants had a rated capacity of 100 MW. Further information about the wind turbines can be found in Appendix A (see Table A2). Additional parameters, such as pitch control gains, are also included. Regarding controllable loads, and assuming that the household sector represents about 30% of total final electricity consumption [12,59], the percentage of controllable loads could then be estimated at around 10% of the global power demand. Recent contributions affirm that, averaged across all countries, space cooling accounted for around 14% of peak demand [60].

Controllable loads were divided into different groups attending to their thermal behaviors. Subsequently, different thermal models were used to estimate their frequency control parameters. In this way, fridges/freezers and electric water heaters were modeled according to Shaad et al. [61], providing different approaches for identification of single-zone lumped parameter thermal models. A direct load control algorithm was used to estimate and forecast the temperature and water usage for each individual water heater. Air-conditioners were modeled based on a detailed energy balance proposed by the authors in [62]. The model has been previously assessed for load management applications under different load performances and conditions. By considering these models, as well as *k*-parameters determined in Equation (6), Table A3 (see Appendix A) summarizes the main configuration parameters according to the different thermal behaviors and customer uses.

4.2. Results

Computer simulations under different operating conditions were carried out using *Matlab-Simulink* environment to evaluate the suitability of both additional control actions counteracting frequency deviations: (i) Two different step load disturbances were considered for Control Area 1

(CA-1), $\Delta P_{L1} = 0.05$ and 0.075 pu; both imbalances remained for 10 min and they were scheduled to disappear after these 10 min of simulation. Control Area 2 remained under balance conditions and non-additional frequency excursions from CA-2 were included in the simulation scenarios. According to the Spanish TSO, different severe situations were collected during the last decade that are in line with the proposed scenarios. Some imbalances were due to wind power curtailments and wind speed oscillations, such as -1.547 MW/min for a 10 min time interval (28 February 2014). Other imbalances were due to special situations, for example a decreasing of 2000 MW for 15 min (3 December 2007) accounting for more than 10% of the power demand. (ii) Different values of the virtual inertia k_{WFs}-factor were also applied: $k_{\mathrm{WFs}} = 0$, 5 and 10. The analysis thus focused on responses under relevant imbalances in one control area, being frequency response under normal operation conditions out of the scope of this paper. A recent discussion including normal operation analysis can be found in [63].

Figure 8 shows the additional wind power contribution to the power system submitted to an under-frequency excursion. The virtual frequency controller made the WTs behave similarly to a conventional synchronous generator during the event, injecting a temporary extra power into the grid. As can be seen, larger k_{WFs}-factor values implied higher amounts of additional power provided by the WTs. Nevertheless, k_{WFs}-factor values had to be within a range of active power temporarily achievable by the WTs according to different constraints. Indeed, excessive k_{WFs}-factor values might lead to additional power values not allowed to be provided by the WTs. Therefore, the k_{WFs}-factor selection process can be considered as a trade-off between an additional inertia provided by the wind resource, i.e., an additional power injected into the power system, and the WT rotational speed deceleration. Contributions focused on low inertia system operation and the relevance of wind turbines to mitigate frequency deviations can be found in [64,65] and in [66] for isolated power systems.

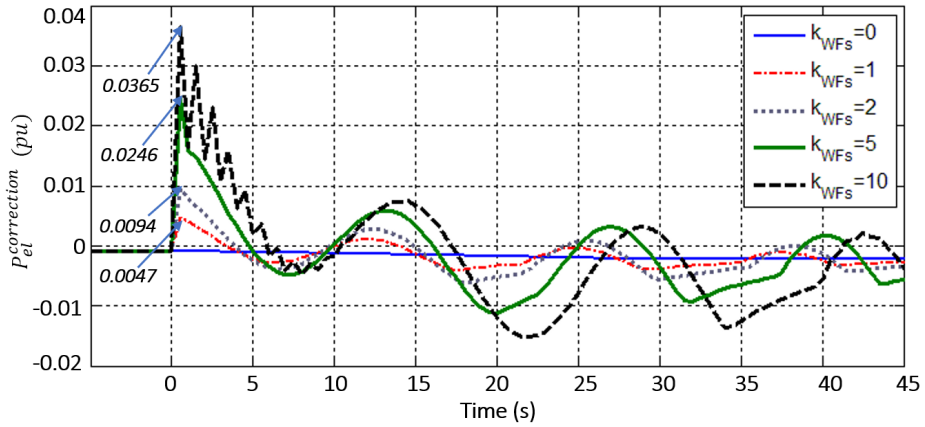

Figure 8. VSWT responses under frequency excursion for different values of the virtual inertia factor (k_{WFs}) and $\Delta P_{L1} = 0.05$.

Figure 9 shows the CA-1 frequency response when demand-side contribution to frequency control was applied (or not), i.e., $\Delta P_{DS} \neq 0$ and $\Delta P_{DS} = 0$, for a series of virtual inertia factor values (k_{WFs}). Results with $\Delta P_{DS} \neq 0$ correspond to simulations where the proposed demand-response frequency control was implemented under different inertia factor values, being $k_{\mathrm{WFs}} = 0$ a scenario where only demand-response was included. According to these results, the maximum value for under-frequency deviation was significantly reduced by 16.6% when only demand-response was considered ($\Delta P_{DS} \neq 0$, $k_{WFs} = 0$). With regard to virtual inertia factors, larger k_{WFs}-factors implied smaller RoCoF values, as a consequence of the additional inertia provided by the WTs to the power system. In this way, decreases of 22.5% and 23.2% were obtained for $k_{WFs} = 5$ and 10, respectively, in comparison to other scenarios without demand-side and WT contribution ($\Delta P_{DS} = 0$, $k_{WFs} = 0$). These aforementioned reduction percentages, i.e., 16.6%, 22.5% and 23.2%, corresponded to a participation share of the controlled load from 40.5% to 44.6%, based on the total available controllable loads. As introduced in

Section 3.2, this percentage of controllable loads varied gradually depending on the severity of the frequency excursion to avoid over-frequency values. In terms of the supply-side frequency response, Figure 10 compares the extra power provided by the CA-1 conventional generating units during the frequency excursion for the different scenarios. This additional active power delivered by conventional generation was significantly reduced when demand and WT frequency response were considered, i.e., maximum peak value was reduced from 0.092 to 0.076 pu. Therefore, this reduction in active power was significant for the presence of demand-side response $\Delta P_{DS} \neq 0$. Additional benefits from virtual inertia factor values ($k_{WFs} \neq 0$) could be achieved by including WT frequency control. This last benefit depended on the wind power capacity considered in the proposed power system. Nevertheless, larger k_{WFs}-factor also reduced the power reserves from the conventional generation units.

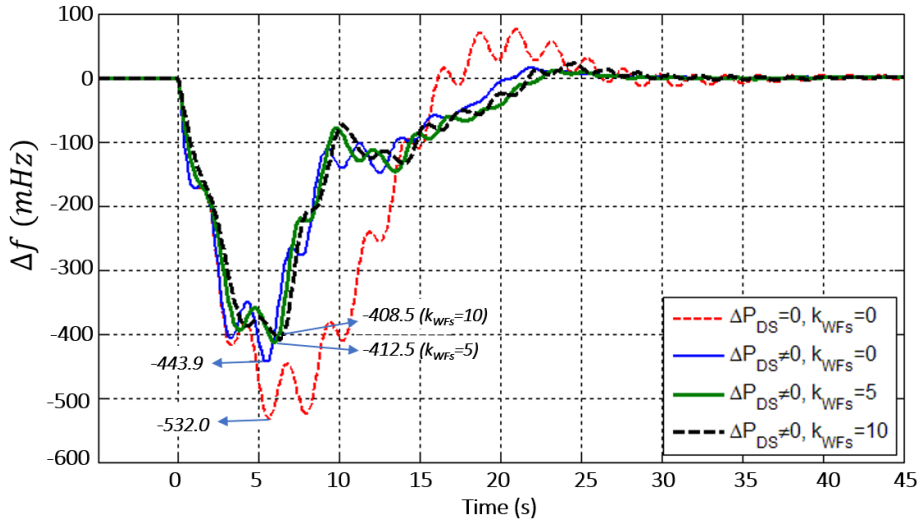

Figure 9. Grid frequency variation for CA-1 (Δf_1) and $\Delta P_{L1} = 0.05$. Comparison of conventional power plant frequency response ($\Delta P_{DS} = 0$, $k_{\mathrm{WFs}} = 0$.) vs. demand-side ($\Delta P_{DS} \neq 0$) and VSWT contribution ($k_{\mathrm{WFs}} \neq 0$).

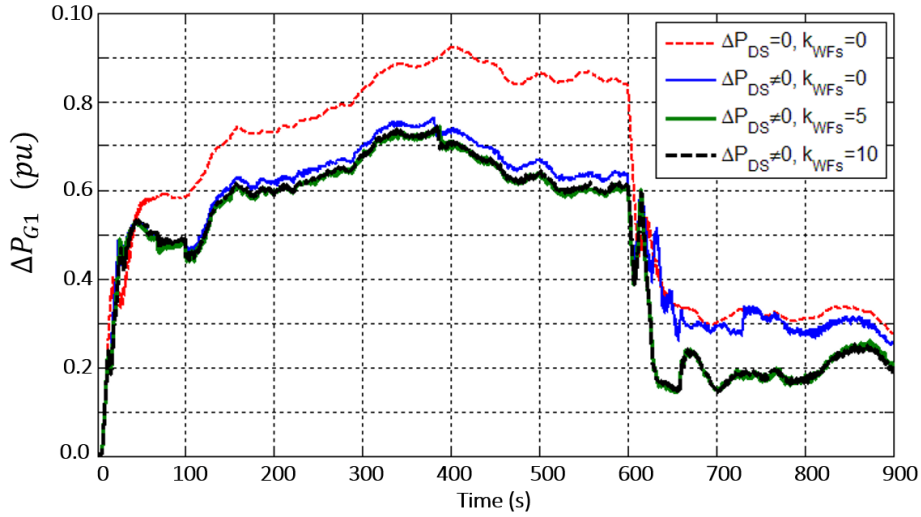

Figure 10. Conventional generation response for CA-1 (ΔP_{G1}) and $\Delta P_{L1} = 0.05$.

With regard to the response of the demand-side frequency control, the participation of the controlled load was linearly distributed from the beginning of the frequency excursion to 10 min. The load controller actions were then spread out along the time of simulation, i.e., 10 min after the disturbance, secondary control response of the controlled load was fully activated. Figure 11

summarizes the contribution to PFC from the controllable loads, $\Delta P_{DS}{}^{PFC}$, for the different simulated scenarios. In line with the proposed load controller described in Section 2.3 (see Figure 4), the demand response was proportional to the frequency excursion, emulating the natural response of conventional generation units. It is worth pointing out that the demand-side contribution to PFC proportionally disappeared with the frequency deviation, as primary response was progressively replaced by the contribution of demand-side to SFC. Figure 12 shows the controlled load responses for the different frequency excursions as regards demand-side contribution to SFC, $\Delta P_{DS}{}^{SFC}$ according to Section 3. Consequently, SFC of controllable loads was implemented by introducing modifications in their thermostat set-point values through Equation (5). Controlled load thermostats were then readjusted, recovering progressively their initial temperature set point values. Figure 13 shows a box-plot of the temperature refrigerator set points, i.e., *Load Group I*, aiming to demonstrate that the temperature variation remained within acceptable limits during the secondary frequency control load participation.

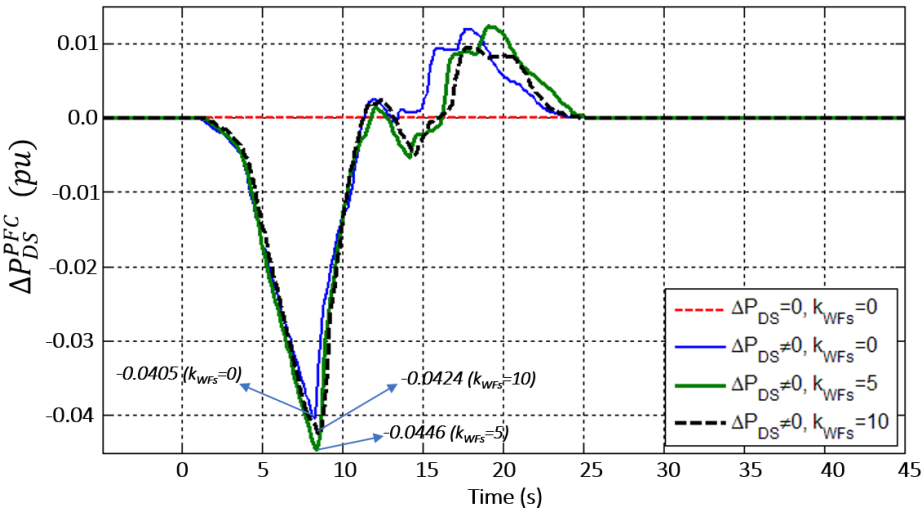

Figure 11. PFC response of controlled loads ($\Delta P_{DS}{}^{PFC}$) when applied to CA-1 and for $\Delta P_{L1} = 0.05$.

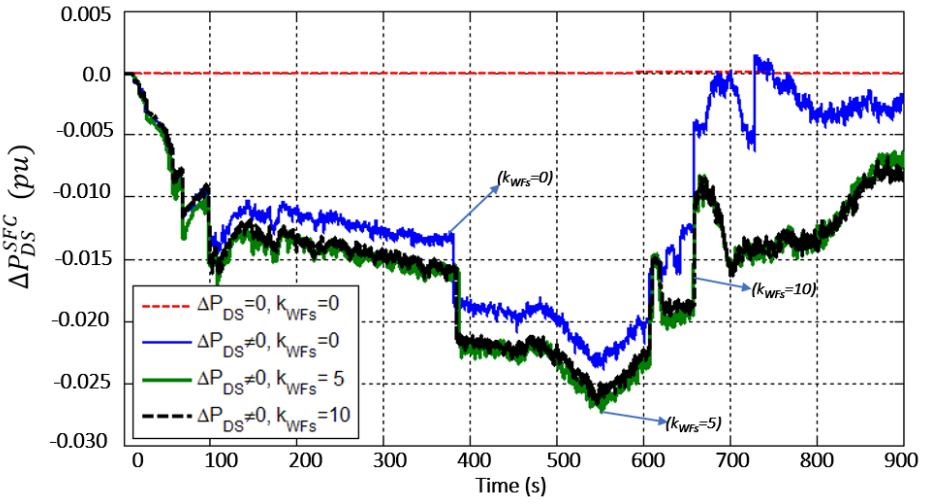

Figure 12. SFC response of controlled loads ($\Delta P_{DS}{}^{SFC}$) when applied to CA-1 and for $\Delta P_{L1} = 0.05$.

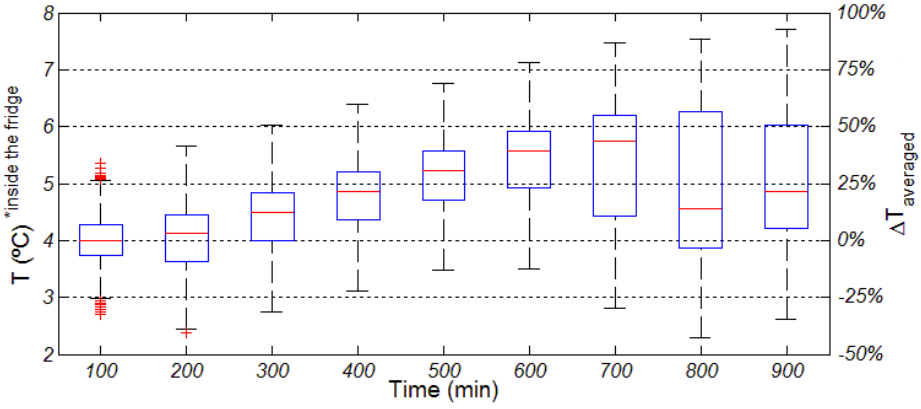

Figure 13. Temperature set point variation for *Load Group I*.

5. Conclusions

An alternative approach to improve dynamic performance of inter-connected power systems with relevant penetration of wind resource is discussed and evaluated. A new frequency control strategy is proposed by introducing demand-side contribution to frequency control, including primary and secondary response under frequency excursions. This demand-side contribution is carried out through the integration of frequency-sensitive load controllers into thermostatically controlled residential loads. Additionally, a supplementary control loop synthesizing virtual inertia for wind power plants is included as well, considering generation rate constraints and a governor dead-band. A combined frequency control strategy is thus proposed and evaluated.

According to the results, frequency deviations were significantly reduced in comparison to classical scenarios by including a combined solution with demand-response and wind power plant participation (peak frequency excursions were reduced by 23%). Similarly, the necessities of both primary and secondary regulation reserves from the supply-side could decrease significantly under power imbalance conditions. From the demand-side, minor effects on the controlled loads were allowed to satisfy minimum comfort levels required by the customers, with set-point temperature variations lower than 2 °C. Consequently, the results show a relevant reduction in supply-side reserve requirements (26.8%) and thus a suitable solution to integrate both controllable loads and wind power plants into the grid frequency stability.

Author Contributions: Data curation, I.M.-B.; Formal analysis, Á.M.-G. and E.G.-L.; Funding acquisition, E.G.-L.; Investigation, A.D.H.; Resources, T.G.-S.; Supervision, Á.M.-G.; Visualization, T.G.-S.; Writing—original draft, A.F.-G.; and Writing—review and editing, Á.M.-G.

Funding: This work was partially supported by by the Regional Seneca Foundation of Spain through the research projects 08747/PI/08 and 19379/PI/14. This work was also supported by project AIM, Ref. TEC2016-76465-C2-1-R (AEI/FEDER, UE).

Acknowledgments: This work was financially supported by the Regional Seneca Foundation of Spain through the research projects 08747/PI/08 and 19379/PI/14.

Conflicts of Interest: The authors declare no conflict of interest.

Abbreviations

The following abbreviations are used in this manuscript:

ACE	Area Control Error
AGC	Automatic Generation Control
CAs	Control Areas
DD	Dynamic demand
DR	Demand response
GDB	Governor Dead-Band
GRC	Generation Rate Constraint
I	Integral
ISE	Integral Squared Error
PFC	Primary frequency control
PI	Proportional Integral
PID	Proportional Integral Derivative
SFC	Secondary frequency control
TCRLs	Thermostatically Controlled Residential Loads
VSWTs	Variable speed wind turbines
WFs	Wind Farms
WT	Wind turbine

Appendix A

Power system and wind turbine parameters for simulations are shown in Tables A1 and A2. Thermal model parameters of controlled residential loads are shown in Table A3.

Table A1. Power system model parameters.

Parameter	Value [PS_1]	Value [PS_2]
Rotational Inertia, H_i [s]	5	7
Damping, D_i [puMW/Hz]	$8.333 \cdot 10^{-3}$	$8.333 \cdot 10^{-3}$
Tie-Line Power Rating, T_{12} [s]	0.0866	0.0866
Speed Regulation, R_i [Hz/puMW]	2.4	9
Integral Controller Gain, K_{Ii} [-]	0.28	0.28
Bias Factor, β_i [puMW/Hz]	0.125	0.150

Table A2. Wind turbine data.

Parameter	Value	Parameter	Value
Nominal power [MW]	2	Rotor inertia [kg · m^2]	$8.6 \cdot 10^6$
Type	VSWT	Generator inertia [kg · m^2]	150
Number of pole pairs	2	Pitch Controller, K_P [-]	2
Gear ratio [-]	96	Pitch Controller, K_I [-]	0.9091
Rotor diameter [m]	80		

Table A3. Thermal model parameters for residential electric loads.

Parameter	Group I	Group II	Group III
T_0, set-point [°C]	2–6	20–26	50–75
T_0, var(0.1) [°C]	4 ^{*appliance}	23.5 ^{*room}	50 ^{*tank}
$\Delta T_{high}/\Delta T_{low}$ [°C]	0.75/-0.75	0.1/-0.1	1.5/-1.5
$t_{on}^{max}/t_{off}^{max}$ [min]	20/20	-/-	28/230

References

1. Huber, M.; Dimkova, D.; Hamacher, T. Integration of wind and solar power in Europe: Assessment of flexibility requirements. *Energy* **2014**, *69*, 236–246. [CrossRef]
2. Simbolotti, G.; Tosato, G.; Kempener, R. *Renewable Energy Integration in Power Grids*; Technical Report; International Renewable Energy Agency (IRENA): Abu Dhabi, UAE, 2015.
3. EURELECTRIC—ENTSO-E Joint Investigation Team. *Deterministic Frequency Deviations—Root Causes and Proposals for Potential Solutions*; EURELECTRIC: Brussels, Belgium, 2011.
4. Wen, T. Load frequency control: Problems and solutions. In Proceedings of the 2011 30th Chinese Control Conference (CCC), Yantai, China, 22–24 July 2011; pp. 6281–6286.
5. Gómez-Expósito, A.; Conejo, A.; Cañizares, C. *Electric Energy Systems: Analisys and Operation*; CRC Press: Boca Raton, FL, USA, 2009.
6. Vijayananda, W.M.T.; Samarakoon, K.; Ekanayake, J. Development of a demonstration rig for providing primary frequency response through smart meters. In Proceedings of the 45th International Universities Power Engineering Conference (UPEC), Cardiff, Wales, UK, 31August–3 September 2010; pp. 1–6.
7. Arghira, N.; Dumitru, I.; Fagarasan, I.; St. Iliescu, S.; Soare, C. Load frequency regulation in power systems. In Proceedings of the IEEE International Conference Automation Quality and Testing Robotics (AQTR), Cluj-Napoca, Romania, 28–30 May 2010; Volume 1, pp. 1–6.
8. European Network of Transmission System Operators for Electricity Union for the Coordination of Transmission of Electricity. *Policy 1—Load-Frequency Control and Performance*; Technical Report; ENTSOE–UCTE: Brussels, Belgium, 2009.
9. Gandhi, N.F.; Mohan, Y.K.; Rao, A.V. Load frequency control of interconnected power system in deregulated environment considering generation rate constraints. In Proceedings of the International Advances in Engineering, Science and Management (ICAESM) Conference, Nagapattinam, Tamil Nadu, India, 30–31 March 2012; pp. 22–25.
10. Chang-Chien, L.R.; Wu, Y.S.; Cheng, J.S. Online estimation of system parameters for artificial intelligence applications to load frequency control. *IET Gener. Transm. Distrib.* **2011**, *5*, 895–902. [CrossRef]
11. Siano, P. Demand response and smart grids—A survey. *Renew. Sustain. Energy Rev.* **2014**, *30*, 461–478. [CrossRef]
12. Cool Appliances. *Policy Strategies for Energy Efficient Homes*; Technical Report; International Energy Agency, IEA: Paris, France, 2003.
13. Ilic, M.D.; Popli, N.; Joo, J.Y.; Hou, Y. A possible engineering and economic framework for implementing demand side participation in frequency regulation at value. In Proceedings of the IEEE Power and Energy Society General Meeting, San Diego, CA, USA, 24–29 July 2011; pp. 1–7.
14. Jay, D.; Swarup, K.S. Frequency restoration using Dynamic Demand Control under Smart Grid Environment. In Proceedings of the IEEE PES Innovative Smart Grid Technologies—India (ISGT India), Kollam, Kerala, India, 1–3 December 2011; pp. 311–315.
15. Douglass, P.J.; Garcia-Valle, R.; Nyeng, P.; Ostergaard, J.; Togeby, M. Demand as frequency controlled reserve: Implementation and practical demonstration. In Proceedings of the 2nd IEEE PES International Innovative Smart Grid Technologies (ISGT Europe) Conference and Exhibition, Manchester, UK, 5–7 December 2011; pp. 1–7.
16. Darby, S. Load management at home: Advantages and drawbacks of some 'active demand side' options. *J. Power Energy* **2012**, *227*, 9–17. [CrossRef]
17. Trudnowski, D.; Donnelly, M.; Lightner, E. Power-System Frequency and Stability Control using Decentralized Intelligent Loads. In Proceedings of the 2006 IEEE PES Transmission and Distribution Conf. and Exhibition, Dallas, TX, USA, 21–24 May 2006; pp. 1453–1459. [CrossRef]
18. Short, J.A.; Infield, D.G.; Freris, L.L. Stabilization of Grid Frequency Through Dynamic Demand Control. *IEEE Trans. Power Syst.* **2007**, *22*, 1284–1293. [CrossRef]
19. Samarakoon, K.; Ekanayake, J. Demand side primary frequency response support through smart meter control. In Proceedings of the 44th International Universities Power Engineering Conference(UPEC), Glasgow, UK, 1–4 September 2009; pp. 1–5.
20. Samarakoon, K.; Ekanayake, J.; Jenkins, N. Investigation of Domestic Load Control to Provide Primary Frequency Response Using Smart Meters. *IEEE Trans. Smart Grid* **2012**, *3*, 282–292. [CrossRef]

21. Molina-García, A.; Bouffard, F.; Kirschen, D.S. Decentralized Demand-Side Contribution to Primary Frequency Control. *IEEE Trans. Power Syst.* **2011**, *26*, 411–419. [CrossRef]
22. Aunedi, M.; Kountouriotis, P.A.; Calderon, J.E.O.; Angeli, D.; Strbac, G. Economic and Environmental Benefits of Dynamic Demand in Providing Frequency Regulation. *IEEE Trans. Smart Grid* **2013**, *4*, 2036–2048. [CrossRef]
23. Pourmousavi, S.A.; Nehrir, M.H. Real-Time Central Demand Response for Primary Frequency Regulation in Microgrids. *IEEE Trans. Smart Grid* **2012**, *3*, 1988–1996. [CrossRef]
24. Zhao, C.; Topcu, U.; Li, N.; Low, S. Design and Stability of Load-Side Primary Frequency Control in Power Systems. *IEEE Trans. Autom. Control.* **2014**, *59*, 1177–1189. [CrossRef]
25. Molina-García, A.; Muñoz Benavente, I.; Hansen, A.; Gomez-Lazaro, E. Demand-Side Contribution to Primary Frequency Control With Wind Farm Auxiliary Control. *IEEE Trans. Power Syst.* **2014**, *29*, 2391–2399. [CrossRef]
26. Tsili, M.; Papathanassiou, S. A review of grid code technical requirements for wind farms. *IET Renew. Power Gener.* **2009**, *3*, 308–332. [CrossRef]
27. Ciupuliga, A.; Gibescu, M.; Fulli, G.; Abbate, A.; Kling, W. Grid Connection of Large Wind Power Plants—A European Overview. In Proceedings of the 8th International Workshop on Large-Scale Integration of Wind Power into Power Systems and Transmission Networks for Offshore Wind Farms, Bremen, Germany, 14–15 October 2009; pp. 349–359.
28. Doherty, R.; Mullane, A.; Nolan, G.; Burke, D.; Bryson, A.; O'Malley, M. An Assessment of the Impact of Wind Generation on System Frequency Control. *IEEE Trans. Power Syst.* **2010**, *25*, 452–460. [CrossRef]
29. Klempke, H.; McCulloch, C.; Wong, A.; Piekutowski, M.; Negnevitsky, M. Impact of high wind generation penetration on frequency control. In Proceedings of the 2010 20th Australasian Universities Power Engineering Conference (AUPEC), Christchurch, New Zealand, 5–8 December 2010; pp. 1–6.
30. Lalor, G.; Mullane, A.; O'Malley, M. Frequency control and wind turbine technologies. *IEEE Trans. Power Syst.* **2005**, *20*, 1905–1913. [CrossRef]
31. Mullane, A.; O'Malley, M. The Inertial Response of Induction-Machine-Based Wind Turbines. *IEEE Trans. Power Syst.* **2005**, *20*, 1496–1503. [CrossRef]
32. Lalor, G.; Ritchie, J.; Rourke, S.; Flynn, D.; O'Malley, M.J. Dynamic frequency control with increasing wind generation. In Proceedings of the IEEE Power Engineering Society General Meeting, Denver, CO, USA, 6–10 June 2004; pp. 1715–1720. [CrossRef]
33. Kou, G.; Till, M.; Bilke, T.; Hadley, S.; Liu, Y.; King, T. Primary Frequency Response Adequacy Study on the U.S. Eastern Interconnection Under High-Wind Penetration Conditions. *IEEE Power Energy Technol. Syst. J.* **2015**, *2*, 125–134. [CrossRef]
34. Johnstone, N.; Hascic, I. Increasing the penetration of intermittent renewable energy: Innovation in energy storage and grid management. In *OECD, Energy and Climate Policy: Bending the Technological Trajectory*; OECD Publishing: Paris, France, 2012; pp. 87–103.
35. Margaris, I.D.; Papathanassiou, S.A.; Hatziargyriou, N.D.; Hansen, A.D.; Sorensen, P. Frequency Control in Autonomous Power Systems With High Wind Power Penetration. *IEEE Trans. Sustain. Energy* **2012**, *3*, 189–199. [CrossRef]
36. *BOE nº 312. Resolution of December 23, 2016, the General Secretariat of Energy, by the Rules for the Electricity Market*; Technical Report; Ministerio de Industria, Turismo y Comercio: Madrid, Spain, 2015. (In Spanish)
37. Wood, A.J.; Wollenberg, B.F. *Power Generation, Operation and Control*; John Wiley & Sons: New York, NY, USA, 1996.
38. Morsali, J.; Zare, K.; Hagh, M. Appropriate generation rate constraint (GRC) modeling method for reheat thermal units to obtain optimal load frequency controller (LFC). In Proceedings of the 5th Conference on Thermal Power Plants (CTPP), Tehran, Iran, 10–11 June 2014; pp. 29–34. [CrossRef]
39. Velusami, S.; Chidambaram, I.A. Decentralized biased dual mode controllers for load frequency control of interconnected power systems considering GDB and GRC non-linearities. *Energy Convers. Manag.* **2007**, *48*, 1691–1702. [CrossRef]
40. Bhatt, P.; Roy, R.; Ghoshal, S.P. GA/particle swarm intelligence based optimization of two specific varieties of controller devices applied to two-area multi-units automatic generation control. *Int. J. Electr. Power Energy Syst.* **2010**, *32*, 299–310. [CrossRef]

41. Rasolomampionona, D.D. A modified power system model for AGC analysis. In Proceedings of the IEEE Bucharest PowerTech, Bucharest, Romania, 28 June–2 July 2009; pp. 1–6.
42. Chen, C.; Zhang, K.; Yuan, K.; Teng, X. Tie-Line Bias Control Applicability to Load Frequency Control for Multi-Area Interconnected Power Systems of Complex Topology. *Energies* **2017**, *10*. [CrossRef]
43. Sheikh, M.R.I.; Muyeen, S.M.; Takahashi, R.; Murata, T.; Tamura, J. Application of self-tuning FPIC to AGC for load frequency control in multi-area power system. In Proceedings of the IEEE Bucharest PowerTech, Bucharest, Romania, 28 June–2 July 2009; pp. 1–7.
44. Sheikh, M.R.I.; Mondol, N. Application of self-tuning FPIC to AGC for Load Frequency Control in wind farm interconnected large power system. In Proceedings of the International Conference on Informatics, Electronics & Vision (ICIEV), Dhaka, Bangladesh, 18–19 May 2012; pp. 812–816.
45. Sheikh, M.R.I.; Takahashi, R.; Tamura, J. Multi-area frequency and tie-line power flow control by coordinated AGC with TCPS. In Proceedings of the International Electrical and Computer Engineering (ICECE) Conference, Dhaka, Bangladesh, 18–20 December 2010; pp. 275–278.
46. Zeni, L.; Rudolph, A.J.; Munster-Swendsen, J.; Margaris, I.; Hansen, A.D.; Sørensen, P. Virtual inertia for variable speed wind turbines. *Wind Energy* **2013**, *16*, 1225–1239. [CrossRef]
47. Morren, J.; Pierik, J.; de Haan, S.W.H. Inertial response of variable speed wind turbines. *Electr. Power Syst. Res.* **2006**, *76*, 980–987. [CrossRef]
48. Ramtharan, G.; Ekanayake, J.B.; Jenkins, N. Frequency support from doubly fed induction generator wind turbines. *IET Renew. Power Gener.* **2007**, *1*, 3–9. [CrossRef]
49. Safdar, M.; Ahmad, M.; Hussain, A.; Lehtonen, M. Optimized residential load scheduling under user defined constraints in a real-time tariff paradigm. In Proceedings of the 17th International Scientific Conference on Electric Power Engineering (EPE), Prague, Czech Republic, 169–18 May 2016; pp. 1–6. [CrossRef]
50. Freris, L.; Infield, D. *Renewable Energy in Power Systems*; John Wiley & Sons, Ltd Registered: Chichester, UK, 2008.
51. Turner, C.; Bining, A.; Gravely, M.; Hope, L.; Oglesby, R.P. *2020 Strategic Analysis of Energy Storage in California*; Technical Report; University of California: Berkeley, CA, USA, 2011.
52. Beil, I.; Hiskens, I.; Backhaus, S. Frequency Regulation From Commercial Building HVAC Demand Response. *Proc. IEEE* **2016**, *104*, 745–757. [CrossRef]
53. Zhang, J.; Domínguez-García, A.D. On the Impact of Measurement Errors on Power System Automatic Generation Control. *IEEE Trans. Smart Grid* **2018**, *9*, 1859–1868. [CrossRef]
54. Masetti, C. Revision of European Standard EN 50160 on power quality: Reasons and solutions. In Proceedings of the 14th International Conference on Harmonics and Quality of Power—ICHQP 2010, Bergamo, Italy, 26–29 September 2010; pp. 1–7. [CrossRef]
55. Tesarova, M.; Nohac, K. Voltage and frequency stability analysis of an island-mode LV distribution network. In Proceedings of the 2014 15th International Scientific Conference on Electric Power Engineering (EPE), Brno, Czech Republic, 12–14 May 2014; pp. 137–142. [CrossRef]
56. Yin, Z.; Che, Y.; Li, D.; Liu, H.; Yu, D. Optimal Scheduling Strategy for Domestic Electric Water Heaters Based on the Temperature State Priority List. *Energies* **2017**, *10*, 1425. [CrossRef]
57. Pipattanasomporn, M.; Kuzlu, M.; Rahman, S.; Teklu, Y. Load Profiles of Selected Major Household Appliances and Their Demand Response Opportunities. *IEEE Trans. Smart Grid* **2014**, *5*, 742–750. [CrossRef]
58. Wai, C.; Beaudin, M.; Zareipour, H.; Schellenberg, A.; Lu, N. Cooling Devices in Demand Response: A Comparison of Control Methods. *IEEE Trans. Smart Grid* **2015**, *6*, 249–260. [CrossRef]
59. Waters, L. *Energy Consumption in the UK*; Technical Report; Dept. for Business, Energy and Industrial Strategy: London, UK, 2017.
60. Motherway, B. *The Future of Cooling Opportunities for Energy-Efficient Air Conditioning*; Technical Report; International Energy Agency: Paris, France, 2018.
61. Shaad, M.; Momeni, A.; Diduch, C.; Kaye, M.; Chang, L. Parameter identification of thermal models for domestic electric water heaters in a direct load control program. In Proceedings of the 25th IEEE Canadian Conf. on Electrical Computer Engineering (CCECE), Montreal, QC, Canada, 29 April–2 May 2012; pp. 1–5. [CrossRef]
62. Molina-Garcia, A.; Gabaldon, A.; Fuentes, J.; Alvarez, C. Implementation and assessment of physically based electrical load models: Application to direct load control residential programmes. *IEE Proc. Gener. Transm. Distrib.* **2003**, *150*, 61–66. [CrossRef]

63. Eriksson, R.; Modig, N.; Elkington, K. Synthetic inertia versus fast frequency response: A definition. *IET Renew. Power Gener.* **2017**, *12*, 514–570. [CrossRef]
64. Gonzalez-Longatt, F. Impact of synthetic inertia from wind power on the protection/control schemes of future power systems: Simulation study. In Proceedings of the 11th IET International Conference on Developments in Power Systems Protection (DPSP 2012), Birmingham, UK, 23–26 April 2012; p. 74.
65. Gonzalez-Longatt, F.; Chikuni, E.; Rashayi, E. Effects of the Synthetic Inertia from wind power on the total system inertia after a frequency disturbance. In Proceedings of the IEEE International Conference on Industrial Technology (ICIT), Cape Town, South Africa, 25–28 February 2013; pp. 826–832. [CrossRef]
66. Delille, G.; Francois, B.; Malarange, G. Dynamic Frequency Control Support by Energy Storage to Reduce the Impact of Wind and Solar Generation on Isolated Power System's Inertia. *IEEE Trans. Sustain. Energy* **2012**, *3*, 931–939. [CrossRef]

© 2019 by the authors. Licensee MDPI, Basel, Switzerland. This article is an open access article distributed under the terms and conditions of the Creative Commons Attribution (CC BY) license (http://creativecommons.org/licenses/by/4.0/).